Modelling the Impact of Sensitivity Distribution Variations of Tetrapolar Impedance Configurations in Microfluidic Analytical Devices

Martin Hantschke, *Member, IEEE,* Iasonas F. Triantis, *Senior Member, IEEE*

***Abstract*— *Goal:* The purpose of this work is to investigate the effects of electrode topology and electrode configuration of tetrapole electrical impedance measurement (TEIM) systems used in microfluidic devices. *Methods:* Two different electrode topologies with fixed dimensions, selected based on reported applications, are investigated. Three dimensional sensitivity maps, generated using finite element modelling (FEM), show fundamental differences in sensitivity distribution between six different injecting and measuring electrode configurations. Transfer impedance values generated for different band sizes and migrating band trains were compared to show the influence of sensitivity distribution on the performance of TEIM used in electrophoresis or cellomics. *Results*: Fundamental differences of sensitivity distribution between different electrode configurations were detected, with "Inline Dipole" and "Square Across" configurations exhibiting areas of negative sensitivity in the tetrapole centre. This causes baseline impedance differences of up to one order of magnitude and effecting the performance when measuring heterogeneous fluids. *Conclusion:* The results suggest that certain electrode configurations should be avoided for applications relying on high spatial resolution. *Significance:* This work demonstrates the significance of impedimetric sensor geometry design in ultimately enabling the miniaturisation of electrophoretic systems towards increasingly portable devices.**

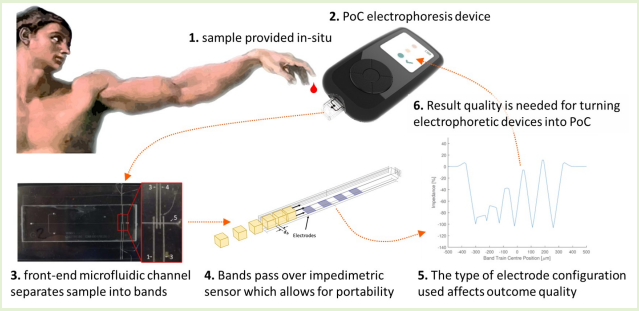

***Index Terms*— Tetrapolar, Impedance, Impedimetric, Sensitivity Distribution, Microfluidics, Electrophoresis.**

I. Introduction

Over the past three decades nano- and micro-structures are being increasingly used in a broad range of analytical techniques such as electrophoresis, liquid chromatography and cellomics [1], [2]. Reducing one or all the dimensions of such a device is mainly aimed at coping with analytical challenges such as small sample volumes, microscopic biological structures but also improves other aspects such as short measurement duration, reduced analyte consumption and downsizing of the device itself, mainly for portability [3], [4].

Besides the commonly used spectrophotometric detection methods, conductivity measurements and impedance spectroscopy are used to investigate the dielectric properties of the bands generated by the analytes present in a sample, offering technically simpler [5] alternative methods that can often achieve lower detection limits [6]. These "impedimetric" methods can be particularly useful in distinguishing analytes that may be optically similar or otherwise not detectable by optical methods, such as carbohydrates [7] and amines [6]. Further advantages of impedimetric methods include the fact that they do not necessitate the use of fluorescent labels, reducing the cumbersome and often hazardous process of attaching labels to the sample [8] and that they allow a high degree of miniaturisation and portability [9], [10]. Bipolar impedance measurements, although simple, present the serious drawback of the high contact impedance of the double layer, i.e. the high impedance of the interface between the surfaces of the electrodes used to measure the sample's dielectric properties and the electrolyte [11]. As the contact impedance is inversely proportional to the electrode area, baseline impedance values often overshadow the sample impedance changes to be measured [11], [12], and that can be more prevalent in microfluidics where small electrodes are used.

A well-established technique to overcome the contribution of the contact impedance to the measurement is to use four electrodes instead of two [11], one pair to apply an AC signal to the sample and one pair to measure its response. This technique is called tetrapolar electrical impedance measurement (termed TEIM) and it minimises the detrimental contribution of the double layer to the measurements [11], making it a very attractive topology for use in microfluidic devices [13].

Still, when using TEIM, one has to consider variations in sensitivity distribution. As detailed in [11] sensitivity describes how much a region within a homogeneous volume conductor

M. Hantschke and I. F. Triantis are with the Research Centre for Biomedical Engineering (RCBE), City, University of London, Northampton Square, London EC1V 0HB, United Kingdom; emails: martin.hantschke.1@city.ac.uk, i.triantis@city.ac.uk

contributes to the measured impedance. Contrary to bipolar impedance measurements, in TEIM areas of negative and positive sensitivity are locally formed, which can give rise to negative or increased positive impedance values and thus cause measurement errors in heterogeneous samples [14]. Given the nature of spatial variations in microfluidics especially for migrating bands of analytes as in electrophoretic separations and cellomics [15], [16], this can potentially lead to misinterpretation of events, creating a significant obstacle for the use of TEIM in such applications. This may be the reason why only a handful of papers have made use of this technique in such applications [13], [17], despite its potential benefits. The sensitivity distribution in TEIM depends highly on the topology of the electrodes [18], [19] as well as the configuration of the injection and measurement electrode pairs [20]. It was shown in [18] that if the inter-electrode distance between the measuring and neighbouring injection sites is reduced, negative sensitivity distribution can be minimised. However even when that distance is small, a region of negative sensitivity still influences measurements close to the electrode surface, which could be particularly detrimental for applications like electrophoresis or cell counting where high spatial resolution is required [21]. Ultimately, it has not still been shown in the literature how detrimental the negative sensitivity really is in TEIM microfluidics; and there is no established method for eliminating it.

In this paper we investigate how impactful sensitivity variations can be in such microfluidic applications; how they affect different band dimensions and localisations; and we assess the usefulness of 6 different electrode configurations, when it comes to microfluidic applications. This can lead to significantly improved TEIM-based microfluidic devices paving the way for portability in microfluidic analytical systems.

II. Theory

When measuring the resistance in linear conductors such as metallic wires the resistance is defined by the specific resistivity of the material (ρ) multiplied with the length of the conductor over the cross-section area [11], while when measuring the resistance of liquids with parallel plate conductivity meters, the spatial component is substituted by the cell constant defined by the distance between electrodes and the area of the plate electrodes [22]. However, in non-uniform volume conductors or electrode topologies other than parallel plate electrodes, the cell constant does not sufficiently describe the experimentally achieved values as it does not account for the contribution of different topologies, frequencies and resistivity changes in the electrode region [23], [24]. It has been suggested that the lead field theory can be used to evaluate the contribution of different regions within the volume conductor to the measured transfer impedance Z by evaluating the sensitivity S [25], as shown by the volume integral in eq. 1:

$$Z = \int_V \rho S dV \tag{1}$$

The sensitivity S is defined as [11]:

$$S = \frac{\overline{J_1} \cdot \overline{J_2}}{I^2} \tag{2}$$

where J_1 is the current density vector in the electrolyte when an external current I is injected through the current injecting and picked up by the voltage measuring electrodes and J_2 the reciprocal current density vector occurring when a unity current is injected through the voltage measuring and picked up by the current injecting electrodes. The current density vectors at a specific point within the volume cannot be directly measured, but by using the principle of reciprocity and the lead field theory in conjunction with finite element modelling the distribution of the sensitivity field within the volume conductor can be calculated [26].

III. Methods

The FEM simulations were carried out using COMSOL Multiphysics v5.3 according to a tutorial by Pettersen et al. [27]. The aim was to assess the performance of different tetrapolar impedimetric configurations in a microfluidic channel, using initially only saline as a homogeneous medium and subsequently adding stationary or migrating analyte “bands”.

A. Simulation Model

The simulation model comprised a saline (NaCl, σ = 1.74 S/m, ϵ_r = 80.1) filled microfluidic channel, embedded in the centre of a 1 mm^3 cube of Polymethylmethacrylate (PMMA, σ = 10^{-19} S/m, ϵ_r = 2.6). The channel was a horizontal parallelepiped of 1 mm length, 70μm width and 50μm height (Fig. 1). These dimensions were based on average values derived from relevant literature [28]–[35]. The injected current was set to the simulation default of 1A at 10kHz frequency after initial runs showed no significant variations over a frequency range of 100Hz - 1MHz. As shown in Fig. 1a and 1b, two tetrapolar electrode topologies were considered: one with four electrodes placed in line with the channel (in-line configuration) and the other featuring two electrode pairs facing each other on either side of the channel (square configuration). The geometrical centres of each topology were made to coincide with that of the channel. The electrodes were designed to be planar and to consist of platinum (Pt, σ = 8.9x10^6 S/m, ϵ_r = 1) with zero thickness. In all configurations the electrodes were designed to extend to the full width of the channel, while each had a length as well as co-planar inter-electrode edge to edge distance respectively of l_e = d_e = 60μm (Fig. 1). Custom (user controlled) meshing was employed to account for the micrometre dimensions of the microfluidic channel but still keep the computational demand at a manageable level. Both, the channel and the surrounding PMMA material were meshed using tetrahedral elements however, a different size mesh was generated for each region. The mesh consists of 39198 element, with minimum quality of 0.2643 and average quality of 0.6898. Each topology was examined using three different connectivity configurations, resulting in six overall configurations. The configurations are listed in Table I with letter I denoting an injecting electrode and letter M denoting a measuring electrode. By reciprocity [11], I and M can be

interchanged, generating the same outcome. The sensitivity distribution in the homogeneous saline volume was calculated through the product of sensitivity and resistivity for each volume element (voxel) of the simulated channel (eq. 1). The simulation data were exported, converted to absolute values and processed using Matlab.

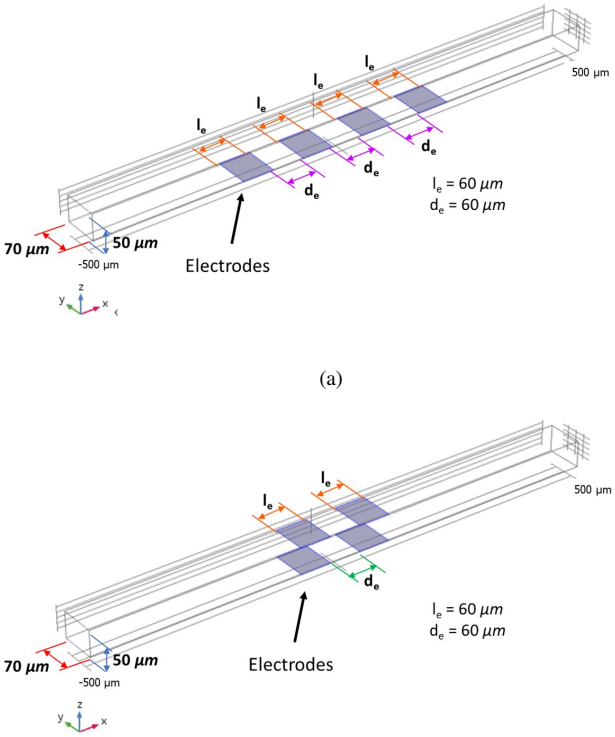

Fig. 1: Electrode Topology, a) Inline topology b) Square topology

TABLE I: Electrode Configuration

Configuration no.	Configuration[1]	Name
i_1	IMMI	Inline Wenner [13]
i_2	MMII	Inline Dipole [18]
i_3	MIMI	Inline Cross [18]
s_1	$M \quad I$ $M \quad I$	Square Across [17]
s_2	$I \quad I$ $M \quad M$	Square Along
s_3	$M \quad I$ $I \quad M$	Square Diagonal

[1] I denotes an injecting and M a measuring electrode

B. Simulation of a variable length stationary band

To understand the impact of the negative and positive sensitivity distribution on samples or analyte bands, such as those found in electrophoresis and cell cytometry, a stationary band with increased conductivity of 3.3 % above baseline [36] was placed in the tetrapole centre (Fig. 2a). Its width and height matched those of the channel, while its length l_b was increased in steps of 10μm from 0μm (no band) to 340μm (beyond the tetrapole dimensions) to include a wide range of realistic band dimensions. For each of the six configurations the band length was varied by applying a parametric sweep study to calculate the resulting transfer impedance.

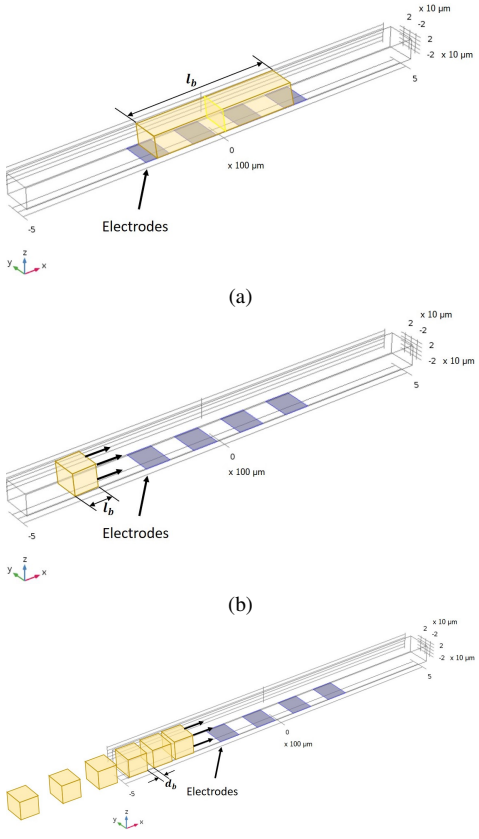

Fig. 2: Methods of investigating the impact of sensitivity distribution on different band measurement scenarios (example images using in-line topology). a) Stationary band (yellow) with varying length l_b = 0μm to 340μm b) Band (yellow) with varied length l_b = 30μm to 230μm, migrating through the channel from x = - 300μm to x = 300μm c) Six bands, equal band length l_b = 70μm and different band distance d_b (10μm, 20μm, 40μm, 60μm and 80μm) are migrating through channel from x= -500μm to x =500μm.

C. Simulation of a variable length migrating band

To evaluate the impact of sensitivity distribution on the detection of a migrating band, the previous procedure was repeated, this time with the band's centre migrating along the channel between x = -300μm to x =300μm as illustrated in Fig. 2b. For each of the six configurations band lengths l_b ranging from 30μm [37] to 230μm [38] were simulated using a parametric sweep study.

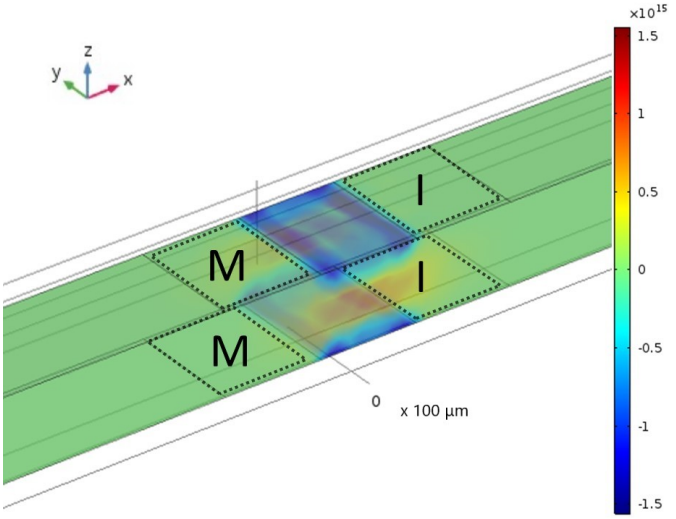

Fig. 3: Three dimensional sensitivity maps of the tetrapole region for configuration s_1. Injecting electrodes (I) and measuring electrodes (M) indicated by dotted squares. Sensitivity distribution indicated in rainbow colour scheme.

D. Simulation of a migrating band train

In a scenario resembling electrophoresis more realistically, a migrating train of six identical bands in different proximities were modelled to assess each configuration's ability to detect and to distinguish each band (Fig. 2c). Each band had a length of 70μm and the distance d_b values between them were 10μm, 20μm, 40μm, 60μm and 80μm. The band train was initially placed at one end (train centre at -500μm) of the channel and migrated to the other end of the channel (train centre at 500μm) passing through the tetrapole centre.

IV. RESULTS AND DISCUSSION

A. Sensitivity distribution in homogeneous solution

In Fig. 3 a 3D plot of configuration s_1 is shown, illustrating the sensitivity distribution (rainbow colour map). As the sensitivity distribution appears uniform in the y axis due to the channel walls, 2 dimensional plots (z-x plane) are used to display the results more clearly. The sensitivity distributions for the six electrode configurations listed in Table I are shown in the two-dimensional plots of Fig. 4. It was observed that some of the six configurations exhibited different ranges of sensitivity values by up to two orders of magnitude. Thus the range of the coloured area was set individually for each plot. For each configuration, positive and negative thresholds were set to one order of magnitude below the absolute maximum value of each of the positive and the negative ranges, respectively. Areas of positive sensitivity values above the positive threshold are coloured orange and areas of negative sensitivity below the negative threshold are coloured green. It can be seen that each distribution depends on the relative position of the injecting and the measuring electrode pairs.

Most of the sensitivity variations of the three inline images (i_1) - (i_3) exhibit similarities to previously reported cases [14], [18]–[20]. For these topologies the sensitivity variations are prominent in regions directly above the inter-electrode areas, with highest absolute sensitivity values at regions close to the electrode edges. Negative sensitivity regions are located between the injecting and measuring electrodes for configuration i_1 (Fig. 4a) and for dipole configuration i_2 (Fig. 4b). However, for configuration i_3 the positive sensitivity location differs from previously reported findings in [20] (Fig. 4c). When it comes to square electrode topologies, the negative and positive sensitivity areas for s_1 are also mostly confined to the inter-electrode regions of the co-planar pairs and extend across the channel's cross-section. For configuration s_2 and s_3 (Fig. 4e and Fig. 4f) mainly positive sensitivity regions are present in the channel centre. However, while the same is true for configuration s_1 close to the channel's central axis, the regions close to the channel's electrode bearing boundaries exhibit negative sensitivity (Figs 4d and 3). The differences of sensitivity distribution between different configurations of identical electrode topologies can be explained by observing closely the angles between the vectors of the neighbouring or overlapping bioelectric fields formed separately by injecting and by measuring electrode pairs. Although the latter are not actively injecting currents they are still considered as injecting pairs when it comes to analysing the sensitivity distribution, according to the reciprocity principle [11].

B. Sensitivity impact on a stationary band

Following the previous observation that sensitivity ranges in the homogeneous solution were varied amongst some configurations, baseline impedance values were calculated. The resulting values exhibited similarities between configurations i_1 & i_3 and s_2 & s_3 which differed significantly from the values of i_2 and s_1, as shown in Table II. The results presented in Fig. 5 show the percentage change of the transfer impedance as a function of the length of the stationary bands positioned at the centre of the tetrapole. The presented data are adjusted to each configuration's baseline – thus all starting at zero - and then normalized to the respective impedance magnitude range (0% when no band present and -100% when band exceeds the tetrapole regions - impedance values are listed in Table II). In terms of form and magnitude of the transfer impedance in the normalised graph, all cases exhibit a decreasing trend as the bands become larger. This is expected because the bands are more conductive than the saline buffer solution and thus as they get larger the impedance drops. Moreover all configurations eventually reach a transfer impedance plateau, reached after the band size exceeds a specific value which is approximately either 200μm or 250μm depending on the tetrapole configuration. We notice that the decrease is not linear in any of the configurations and there are three different trends evident corresponding to pairs of them, namely i_1 & i_3, i_2 & s_1 and s_2 & s_3.

More specifically, configurations i_2 & s_1 exhibit erroneous positive values relative to their starting baseline value when the band is sized between 10 μm - 120μm - peaking at 60μm - as these band sizes coincide with negative sensitivity regions. They also exhibit very small variations for small band lengths, even with the normalised values, and thus they

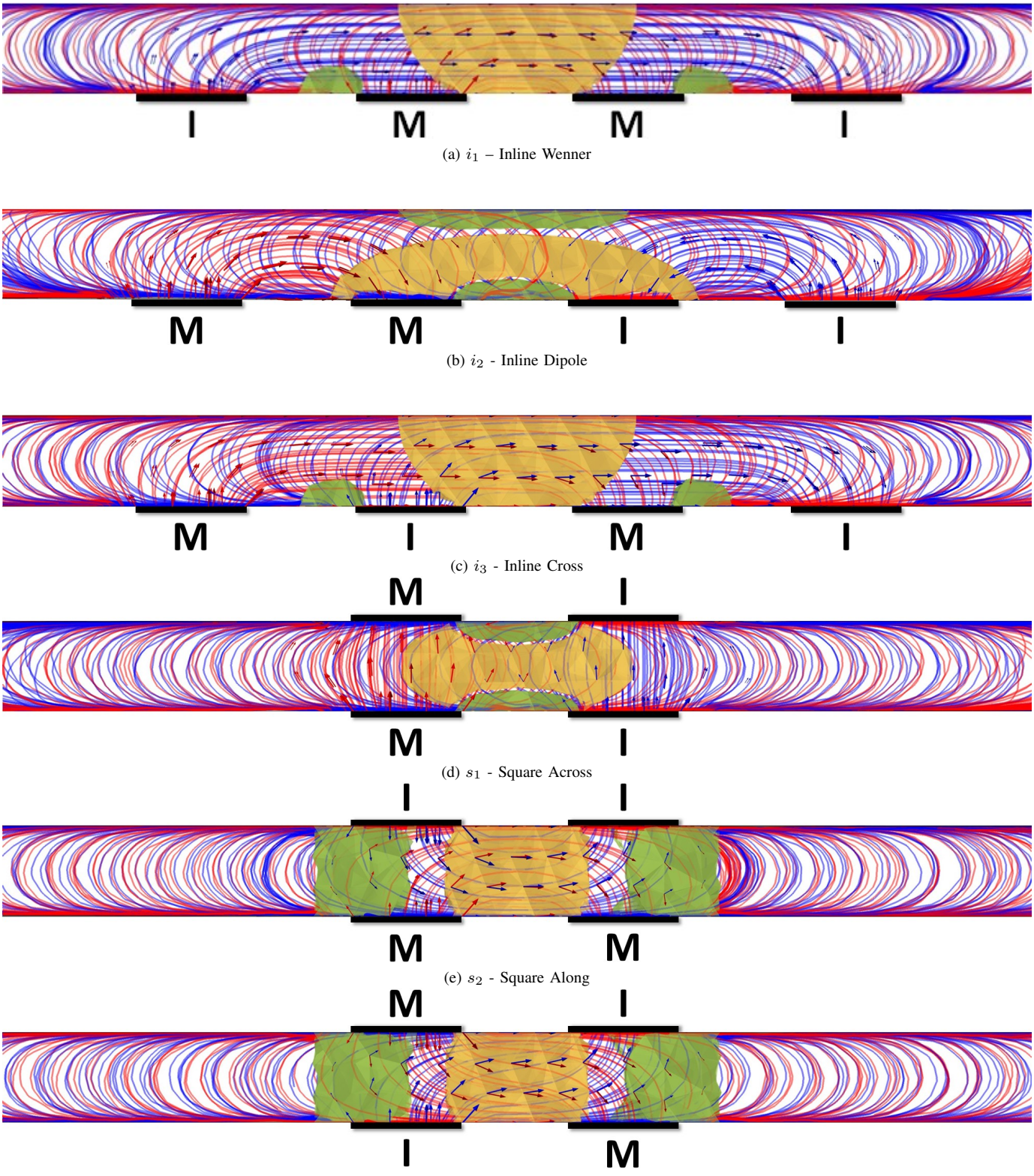

(a) i_1 – Inline Wenner

(b) i_2 - Inline Dipole

(c) i_3 - Inline Cross

(d) s_1 - Square Across

(e) s_2 - Square Along

(f) s_3 - Square Diagonal

Fig. 4: Side view of the sensitivity distribution and current density vectors for the region from x = -250 μm to x = 250 μm in the z-x plane. Orange area = positive sensitivity distribution, green area = negative sensitivity distribution, Red lines and arrows = current density vector J_1, Blue lines and arrows = current density vector J_2

are not appropriate for small bands. Configurations s_2 & s_3 exhibit approximately linear impedance change with length increase until the band reaches 50μm, i.e. for lengths that are approximately within the area between the measurement

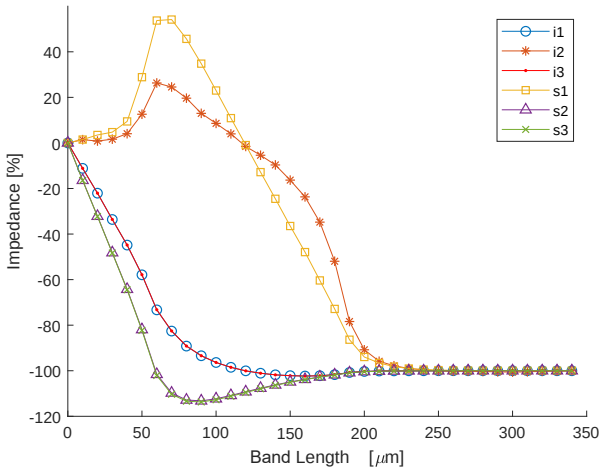

Fig. 5: Calculated percentage impedance change for a stationary band in the tetrapole centre, as indicated in Fig. 2a, and with length varying from 0μm to 340μm.

TABLE II: Impedance values for variable length stationary bands

Configuration no.	Baseline Impedance[2]	Impedance Range[3]
i_1	15.2 kΩ	485 Ω
i_2	1.36 Ω	0.04 Ω
i_3	15.21 kΩ	486 Ω
s_1	24.99 Ω	0.80 Ω
s_2	10.2 kΩ	326.2 Ω
s_3	10.17 kΩ	324.7 Ω

[2] *Value obtained when no band was present.*

[3] *Value in excess of baseline, with band exceeding tetrapole region*

electrodes. However, their absolute responses then exceed the $|-100\%|$ value, reaching higher absolute impedance values for intermediate size bands between 60μm and 200μm band length due to overlap with areas of positive sensitivity. Finally, configurations i_1 & i_3 exhibit a less steep decrease for band lengths within the sensing area but do not exceed the starting-ending values of their respective normalised ranges, thus exhibiting a more predictable impedance-band length relationship characteristic. Also, configurations s_2 & s_3 reach their maximum impedance range at 60μm; i_1 & i_3 at 120μm; while configurations i_2 & s_1 do that at about 240μm. Overall, these results indicate that the positive and negative sensitivity regions have an impact on the detection of bands whose length overlaps with the sensing region.

C. Sensitivity impact on a single migrating band

Fig. 6 illustrates the simulated electropherograms of single bands of various lengths migrating along the channel through the tetrapole centre, with each subplot corresponding to a different configuration. Similar to Fig. 5 plots are adjusted to each configuration's baseline – thus all starting at zero - and then normalized to the respective impedance magnitude range. All band lengths simulated with configurations i_1 & i_3 (Fig. 6a and 6c respectively) resemble Gaussians, similar to those in typical electropherograms [7]. Bands shorter or slightly larger than the 60μm inter-electrode distance do not reach the full normalised range, while longer ones are reaching a plateau at the full impedance magnitude with the length of the plateau increasing with the band length. Minimal (1.2 %) overshoot around the baseline and plateau due to sensitivity variations on the respective borders between negative and positive sensitivity regions are recorded.

For configurations i_2 & s_1 (Fig. 6b and 6d respectively) migrating bands exhibit a negative leading and tailing peak of 62% & 72% respectively. Band lengths up to 110μm exhibit positive impedance peaks, falsely suggesting band concentration decrease. For band lengths larger than $2 \times d_e$ the impedance change is shown on average to be negative as expected, however the leading and tailing peaks present an overall distorted band form. The peaks recorded for configurations s_2 & s_3 resemble the forms of i_1 & i_3, but even with the smaller band lengths being more distinguishable or - down to 70μm - reaching the full impedance range (Fig. 6e and 6f respectively). However, they reach values that exceed the full range at the baseline and plateau (6.2 %) - significantly larger than in configurations i_1 & i_3 - which can lead to quantitative errors especially for shorter band lengths.

The recorded peaks displayed in Fig. 6 represent spatial electropherograms of different size bands. It is common to use the full width at half max (FWHM) of spatial or temporal peaks to assess the efficiency of an electrophoretic system [39]. To evaluate the performance of the different configurations, the data in Fig. 7 have been derived by calculating the ratio of each band's length l_b to the FWHM of the corresponding migrating band of Fig. 6. This value, as percentage, expresses how accurately each band length is detected by each configuration, with a value of 100% being the optimal. A value lower than 100% means that the electrophoretic system suffers efficiency loss due to the sensor performance, which should be avoided. Fig. 7 shows that i_1 & i_3 as well as s_2 & s_3 all accurately represent bands of sizes longer than 70 μm, however they suffer a reduction in accuracy for band sizes of 70 μm and shorter down to 35% and 42% respectively. The accuracy of s_2 & s_3 for shorter bands declines less steeply making this topology superior to i_1 & i_3 as it can detect shorter bands without a loss in efficiency of the electrophoretic system. Similarly to conventional optical sensors the detector output depends on size of the detection window [39]. This is equivalent to the size of the positive sensitivity region in the tetrapole centre and depends mainly on electrode geometry of the measurement electrodes, as shown by our work in [40]. Although values for i_2 & s_1 have been included in Fig. 7 these have to be considered with caution as the sum of the multiple peak widths has been used in the assessment. The general signal distortion does not allow for direct assessment of efficiency of the electrophoretic system by these means. Based on the above results, configurations i_1, i_3, s_2 and s_3 can be used in applications such as electrophoresis. The first two are preferable for quantitative measurements of longer bands, whereas the latter two should be used for applications

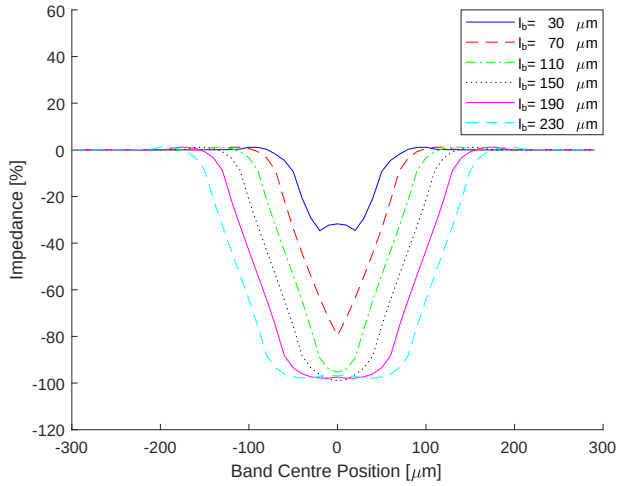

(a) i_1 – Inline Wenner

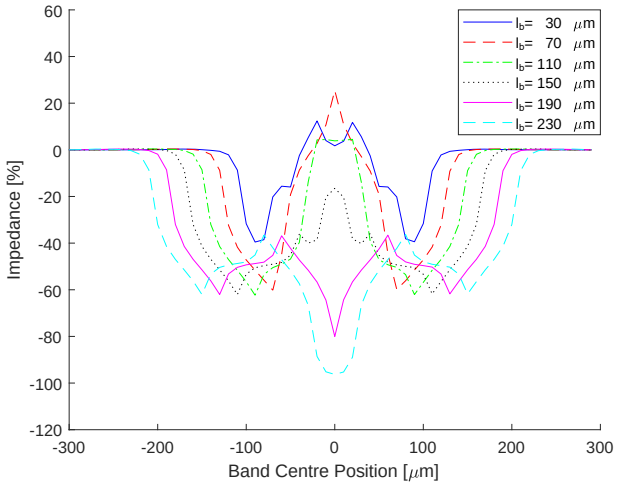

(b) i_2 - Inline Dipole

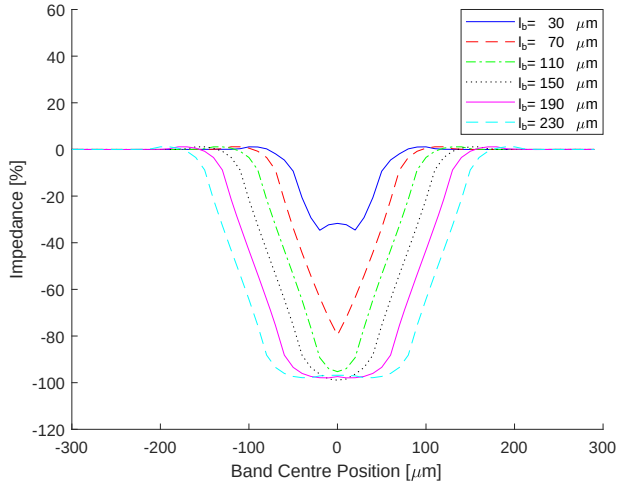

(c) i_3 - Inline Cross

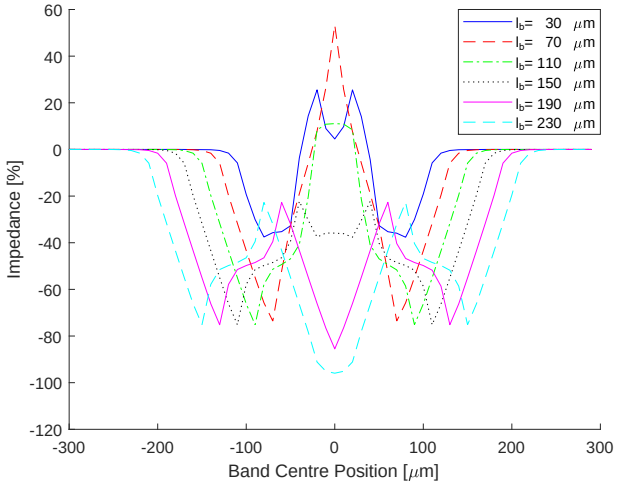

(d) s_1 - Square Across

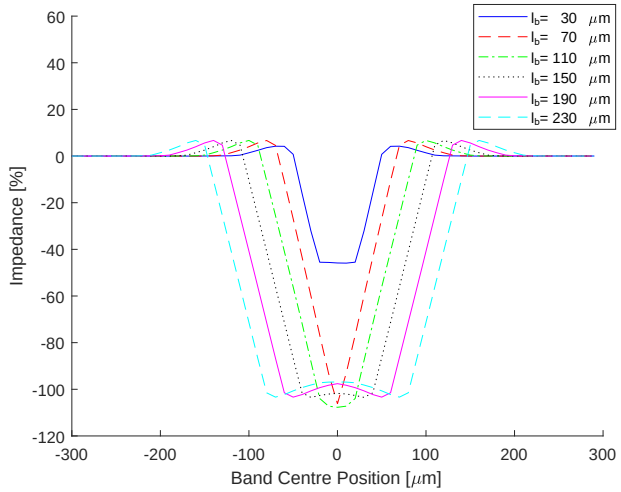

(e) s_2 - Square Along

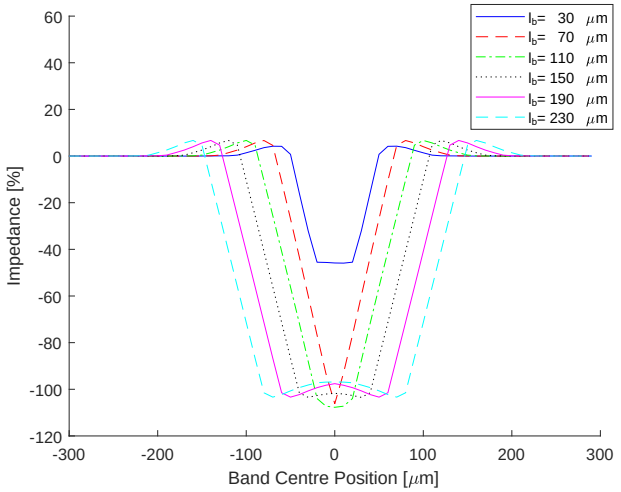

(f) s_3 - Square Diagonal

Fig. 6: Impedance change normalized to baseline and range for a single band migrating through mircofluidic channel from x = -300μm to x =300μm as indicated in Fig. 2b. Six bands with different length l_b = 30μm to 230μm per electrode configuration.

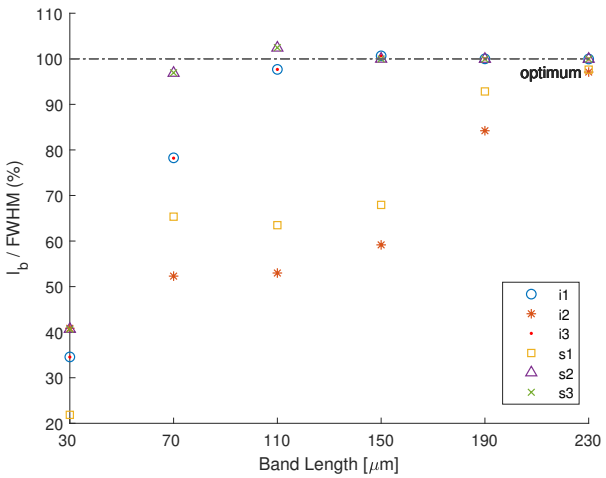

Fig. 7: Detector accuracy as ratio of length l_b of the migrating band and full peak width at half maximum (FWHM) in percent. The black dashed line at 100% is the optimum accuracy defined as accuracy where the detector signal represents the length of the migrating band.

where higher spatial resolution is needed. Configurations i_2 & s_1 should be avoided or used with caution, as only large band lengths are somewhat quantitatively represented.

D. Sensitivity impact on a migrating band train

Each configuration's simulated electropherogram of a train of six consecutive bands of variable spacing exhibits fundamental differences in magnitude, number and location of the recorded peaks, as illustrated in Fig. 8. Whereas configurations i_1 & i_3 (Fig. 8a and 8c respectively) generate the correct locations for the (negative) peaks, the first four peaks from the left (with inter-band spacing of d_b = 10μm, d_b = 20μm and d_b = 40μm) are merging together creating erroneous additional peaks with increased negative impedance due to the overlap of bands in regions of positive sensitivity. The reduced magnitude (79%) recorded for each peak is due to the band lengths being 70μm similar to the impedance exhibited by single bands of that length in Figs. 6a and 6c. For configurations i_2 & s_1 (Fig. 8b and 8d respectively) the first 3 to 4 bands are not distinguishable due to multiple peaks caused by regions of positive and negative sensitivity. Bands 5 and 6 exhibit positive impedance due to negative sensitivity in the tetrapole centre. The overlap of bands in regions of positive sensitivity outside the tetrapole centre result in additional negative impedance peaks, potentially leading to misinterpretation of the electropherogram. Finally, configurations s_2 & s_3 (Fig. 8e and 8f respectively) exhibit peaks at the correct locations, corresponding to the bands. All 6 peaks are distinguishable, however the first three peaks are nearly merging with one another exhibiting slightly reduced magnitude and limited spatial resolution due to negative sensitivity areas affecting the adjacent bands. The remaining peaks show increased magnitude to 106 % in accordance to Fig. 5 as well as positive overshoot as presented in Fig. 6e and 6f. Trains of bands migrating through the tetrapole centre at close proximity ($d_b < d_e$) proves to be challenging for all configurations with configurations i_1 & i_3 producing false peaks and configurations i_2 & s_1 generating an inconclusive outcome altogether. Configurations s_2 & s_3 produce the best results in terms of spatial resolution.

V. Conclusion

Negative and positive sensitivity distributions were shown to potentially have substantial impact in microfluidic applications like electrophoresis when the analyte bands are detected using tetrapolar electrical impedance rather than optical fluorescence sensing. Sensitivity distribution variations resulted to notable performance differences between some of the electrode configurations assessed in this paper. Starting with a homogeneous volume, with saline used as the microfluidic channel's buffer solution, significant baseline impedance differences were observed between three pairs of the assessed configurations. This indicates that, independent of their sensitivity distribution characteristics, two of these configurations – namely i_2 & s_1 - may prove to be more challenging than others when used experimentally, because they exhibit a lower impedance range. Thus, higher amplification will be required making these setups more prone to signal degradation by noise or interference.

When analytes were simulated the aforementioned two configurations performed poorly in terms of the resulting impedance variations relative to the band length; detection of small bands; the electropherogram shape; and the configurations' ability to distinguish between bands in a train migrating along the channel. The remaining configurations are also affected - albeit much less - by negative and positive sensitivity distribution inhomogeneities as these can cause potential errors in the detection of small bands in relation to the sensor area. Limitations are also exposed for detection of consecutive bands in a train migrating at close distance. Generally, inline configurations i_1 & i_3 can be recommended for applications that involve relatively large bands and that require accurate quantification. Between these two configurations i_1 is preferable as it allows more flexibility in adjusting the geometry of the measurement electrode pair for a particular application without affecting the location of the injecting electrodes. Square configurations s_2 & s_3, which may be more difficult to fabricate, are recommended for applications where spatial resolution is important. Their performance is identical, making either of them the optimum choice.

Acknowledgment

The authors would like to thank Genetic Microdevices Ltd. for financial and technical support.

References

[1] E. R. Castro and A. Manz, "Present state of microchip electrophoresis: State of the art and routine applications," *Journal of Chromatography A*, vol. 1382, pp. 66–85, 2015.

[2] H. Andersson and A. van den Berg, "Microfluidic devices for cellomics: a review," *Sensors and Actuators B: Chemical*, vol. 92, no. 3, pp. 315–325, 2003.

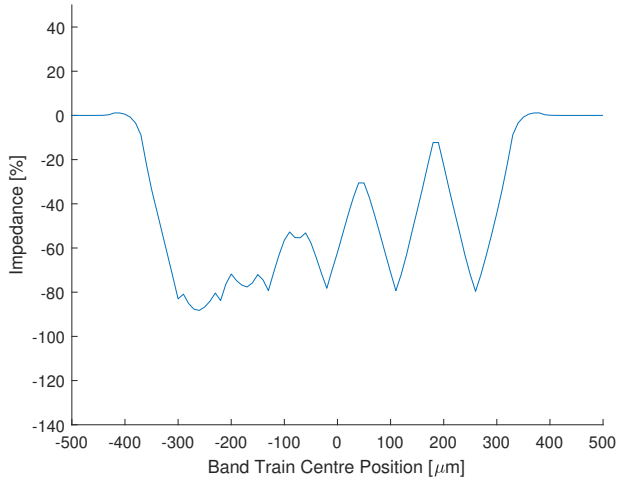

(a) i_1 – Inline Wenner

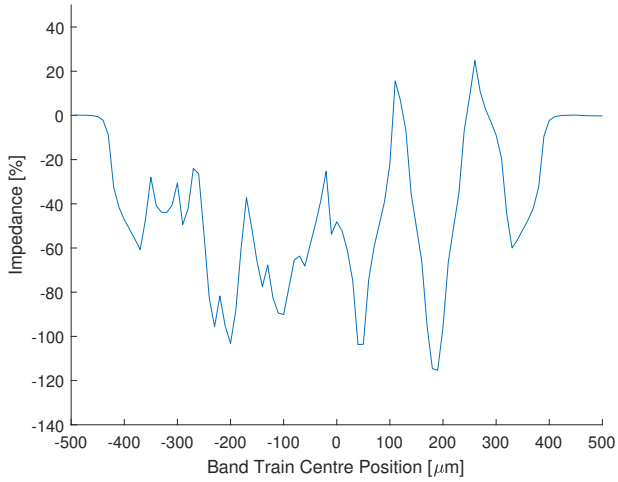

(b) i_2 - Inline Dipole

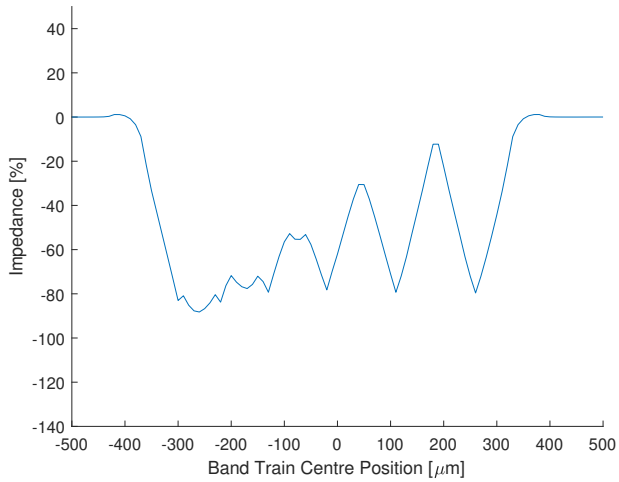

(c) i_3 - Inline Cross

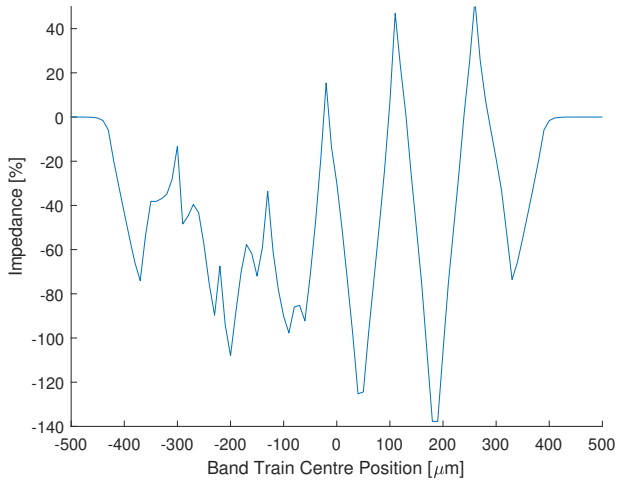

(d) s_1 - Square Across

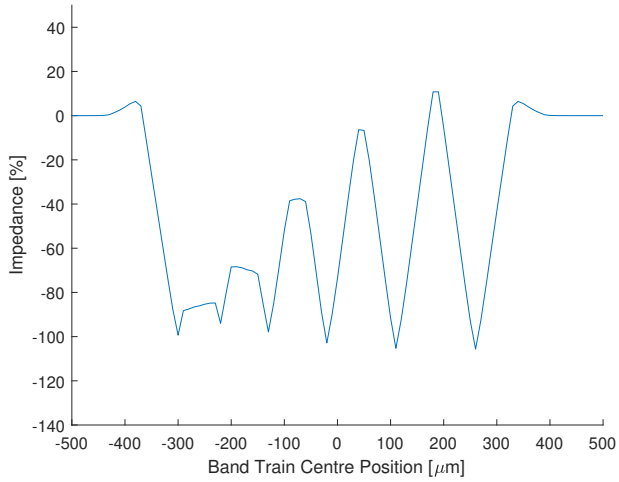

(e) s_2 - Square Along

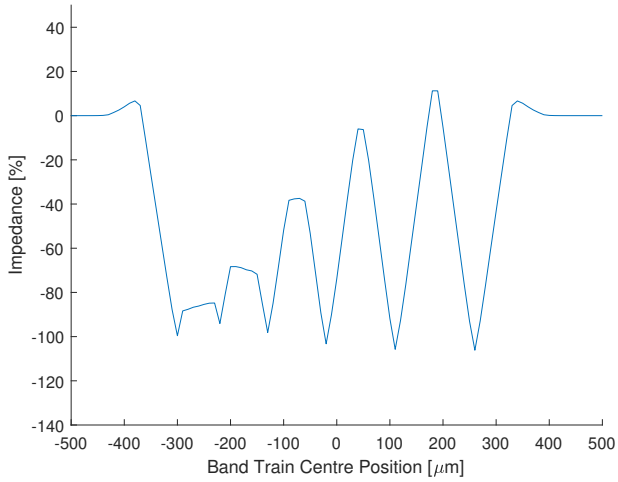

(f) s_3 - Square Diagonal

Fig. 8: Impedance change normalized to baseline and range for six consecutive bands with equal length l_b = 70μm migrating through the mircofluidic channel from x = -500μm to x = 500μm as indicated in Fig. 2c. Distance between each band d_b = 10μm, 20μm, 40μm, 60μm, 80μm.

[3] P. S. Dittrich and A. Manz, "Lab-on-a-chip: microfluidics in drug discovery," *Nature Reviews Drug Discovery*, vol. 5, no. 3, pp. 210–218, 2006.

[4] D. Janasek, J. Franzke, and A. Manz, "Scaling and the design of miniaturized chemical-analysis systems," *Nature*, vol. 442, no. 7101, pp. 374–380, 2006.

[5] A. J. Zemann, "Conductivity detection in capillary electrophoresis," *TrAC Trends in Analytical Chemistry*, vol. 20, no. 6, pp. 346 – 354, 2001.

[6] X. Y. Gong and P. C. Hauser, "Determination of different classes of amines with capillary zone electrophoresis and contactless conductivity detection," *Electrophoresis*, vol. 27, no. 2, pp. 468–473, 2006.

[7] C. W. Klampfl, M. Himmelsbach, and W. Buchberger, "Analysis of Simple Carbohydrates by Capillary Electrophoresis and Capillary Electrophoresis–Mass Spectrometry," in *Capillary Electrophoresis of Carbohydrates: From Monosaccharides to Complex Polysaccharides*, N. Volpi, Ed. Totowa, NJ: Humana Press, 2011, pp. 1–21.

[8] P. R. Reddy and N. Raju, "Gel Electrophoresis - Principles and Basics," in *Gel-Electrophoresis and Its Applications*, S. Magdeldin, Ed. Rijeka: IntechOpen, 2012, pp. 15–32.

[9] P. Kassanos, L. Constantinou, I. F. Triantis, and A. Demosthenous, "An Integrated Analog Readout for Multi-Frequency Bioimpedance Measurements," *IEEE Sensors Journal*, vol. 14, no. 8, pp. 2792 – 2800, 2014.

[10] J. J. P. Mark, R. Scholz, and F.-M. Matysik, "Electrochemical methods in conjunction with capillary and microchip electrophoresis," *Journal of Chromatography A*, vol. 1267, pp. 45–64, 2012.

[11] S. Grimnes and G. Martinsen, *Bioimpedance and Bioelectricity Basics*, 2nd ed. New York: Academic Press, 2008.

[12] J. G. A. Brito-Neto, J. A. Fracassi da Silva, L. Blanes, and C. L. do Lago, "Understanding Capacitively Coupled Contactless Conductivity Detection in Capillary and Microchip Electrophoresis. Part 1. Fundamentals," *Electroanalysis*, vol. 17, no. 13, pp. 1198–1206, 2005.

[13] R. M. Guijt, C. J. Evenhuis, M. Macka, and P. R. Haddad, "Conductivity detection for conventional and miniaturised capillary electrophoresis systems," *Electrophoresis*, vol. 25, no. 23-24, pp. 4032–4057, 2004.

[14] S. Grimnes and G. Martinsen, "Sources of error in tetrapolar impedance measurements on biomaterials and other ionic conductors," *Journal of Physics D: Applied Physics*, vol. 40, no. 1, pp. 9–14, 2006.

[15] G. W. Slater, C. Desruisseaux, and S. J. Hubert, "DNA Separation Mechanisms During Electrophoresis," in *Capillary Electrophoresis of Nucleic Acids. Methods in Molecular Biology*, K. R. Mitchelson and J. Cheng, Eds. Totowa, NJ: Humana Press, 2001, pp. 27–41.

[16] C. Canali, A. Heiskanen, H. B. Muhammad, P. Høyum, F. J. Pettersen, M. Hemmingsen, A. Wolff, M. Dufva, O. G. Martinsen, and J. Emnéus, "Bioimpedance monitoring of 3D cell culturing-Complementary electrode configurations for enhanced spatial sensitivity," *Biosensors and Bioelectronics*, vol. 63, pp. 72–79, 2015.

[17] K. A. Mahabadi, I. Rodriguez, C. Y. Lim, D. K. Maurya, P. C. Hauser, and N. F. De Rooij, "Capacitively coupled contactless conductivity detection with dual top-bottom cell configuration for microchip electrophoresis," *Electrophoresis*, vol. 31, no. 6, pp. 1063–1070, 2010.

[18] P. Kassanos, A. Demosthenous, and R. H. Bayford, "Towards an optimized design for tetrapolar affinity-based impedimetric immunosensors for lab-on-a-chip applications," in *2008 IEEE-BIOCAS Biomedical Circuits and Systems Conference, BIOCAS 2008*, 2008, pp. 141–144.

[19] F. N. Moretti, J. L. Cabrera, and R. E. Madrid, "Zonal selectivity by sensitivity modulation in linear tetrapolar impedance sensors," *Sensors and Actuators, B: Chemical*, vol. 255, pp. 1268–1275, 2018.

[20] P. Kassanos, A. Demosthenous, and R. H. Bayford, "Comparison of tetrapolar injection-measurement techniques for coplanar affinity-based impedimetric immunosensors," in *2008 IEEE-BIOCAS Biomedical Circuits and Systems Conference, BIOCAS 2008*, 2008, pp. 317–320.

[21] A. M. Bond, "Past, present and future contributions of microelectrodes to analytical studies employing voltammetric detection. A review," *Analyst*, vol. 119, no. 11, pp. 1–21, 1994.

[22] H. Ma, Y. Su, and A. Nathan, "Cell constant studies of bipolar and tetrapolar electrode systems for impedance measurement," *Sensors and Actuators B: Chemical*, vol. 221, pp. 1264–1270, 2015.

[23] P. Tůma, F. Opekar, and K. Štulik, "A contactless conductivity detector for capillary electrophoresis: Effects of the detection cell geometry on the detector performance," *Electrophoresis*, vol. 23, no. 21, pp. 3718–3724, 2002.

[24] B. Graß, D. Siepe, A. Neyer, and R. Hergenröder, "Comparison of different conductivity detector geometries on an isotachophoresis PMMA-microchip," *Fresenius' Journal of Analytical Chemistry*, vol. 371, no. 2, pp. 228–233, 2001.

[25] D. B. Geselowitz, "An Application oF Electrocardiographic Lead Theory to Impedance Plethysmography," *IEEE Trans. Biomed. Eng.*, vol. BME-18, no. 1, pp. 38–41, 1971.

[26] B. H. Brown, A. J. Wilson, and P. Bertemes-Filho, "Bipolar and tetrapolar transfer impedance measurements from volume conductor," *Electronics Letters*, vol. 36, no. 25, pp. 2060–2062, 2000.

[27] F.-J. Pettersen and J. O. Høgetveit, "From 3D tissue data to impedance using Simpleware ScanFE+IP and COMSOL Multiphysics – a tutorial," *Journal of Electrical Bioimpedance*, vol. 2, no. 1, pp. 13–32, 2011.

[28] D. Kaniansky, M. Masár, R. Bodor, M. Zúborová, E. Olvecká, M. Jöhnck, and B. Stanislawski, "Electrophoretic separations on chips with hydrodynamically closed separation systems." *Electrophoresis*, vol. 24, no. 12-13, pp. 2208–27, 2003.

[29] M. Galloway, W. Stryjewski, A. Henry, S. M. Ford, S. Llopis, R. L. Mccarley, and S. A. Soper, "Contact Conductivity Detection in Poly (methyl methacylate) -Based Microfluidic Devices for Analysis of Mono- and Polyanionic Molecules," *Analytical Chemistry*, vol. 74, no. 10, pp. 2407–2415, 2002.

[30] H. Shadpour, M. L. Hupert, D. Patterson, C. Liu, M. Galloway, W. Stryjewski, J. Goettert, and S. A. Soper, "Multichannel microchip electrophoresis device fabricated in polycarbonate with an integrated contact conductivity sensor array," *Analytical Chemistry*, vol. 79, no. 3, pp. 870–878, 2007.

[31] S. D. Noblitt, L. C. Staicu, C. J. Ackerson, and C. S. Henry, "Sensitive, Selective Analysis of Selenium Oxoanions Using Microchip Electrophoresis with Contact Conductivity Detection," *Analytical Chemistry*, vol. 86, no. 16, pp. 8425–8432, 2014.

[32] X. Bai, C. Roussel, H. Jensen, and H. H. Girault, "Polyelectrolyte-modified short microchannel for cation separation," *Electrophoresis*, vol. 25, no. 6, pp. 931–935, 2004.

[33] X. Bai, Z. Wu, J. Josserand, H. Jensen, H. Schafer, and H. H. Girault, "Passive conductivity detection for capillary electrophoresis," *Analytical Chemistry*, vol. 76, no. 11, pp. 3126–3131, 2004.

[34] S. Staal, M. Ungerer, A. Floris, H. W. Ten Brinke, R. Helmhout, M. Tellegen, K. Janssen, E. Karstens, C. van Arragon, S. Lenk, E. Staijen, J. Bartholomew, H. Krabbe, K. Movig, P. Dubský, A. van den Berg, and J. Eijkel, "A versatile electrophoresis-based self-test platform," *Electrophoresis*, vol. 36, no. 5, pp. 712–721, 2015.

[35] E. X. Vrouwe, R. Luttge, and A. van den Berg, "Direct measurement of lithium in whole blood using microchip capillary electrophoresis with integrated conductivity detection," *Electrophoresis*, vol. 25, no. 10-11, pp. 1660–1667, 2004.

[36] W. Thormann, M. C. Breadmore, J. Caslavska, and R. A. Mosher, "Dynamic computer simulations of electrophoresis: A versatile research and teaching tool," *Electrophoresis*, vol. 31, no. 5, pp. 726–754, 2010.

[37] D. Bottenus, T. Z. Jubery, Y. Ouyang, W. J. Dong, P. Dutta, and C. F. Ivory, "10000-fold concentration increase of the biomarker cardiac troponin i in a reducing union microfluidic chip using cationic isotachophoresis," *Lab on a Chip*, vol. 11, no. 5, pp. 890–898, 2011.

[38] H. Cui, P. Dutta, and C. F. Ivory, "Isotachophoresis of proteins in a networked microfluidic chip: Experiment and 2-D simulation," *Electrophoresis*, vol. 28, no. 7, pp. 1138–1145, 2007.

[39] S. D. Noblitt and C. S. Henry, "Overcoming Challenges in Using Microchip Electrophoresis for Extended Monitoring Applications," in *Capillary Electrophoresis and Microchip Capillary Electrophoresis*, C. D. García, K. Y. Chumbimuni-Torres, and E. Carrilho, Eds. John Wiley & Sons, Ltd, 2013, pp. 177–200.

[40] M. Hantschke, D. Sideris, P. A. Kyriacou, and I. F. Triantis, "Optimization of Tetrapolar Impedance Electrodes in Microfluidic Devices for Point of Care Diagnostics using Finite Element Modeling," in *Proceedings of the Annual International Conference of the IEEE Engineering in Medicine and Biology Society, EMBS*, vol. 2018-July, 2018, pp. 5321–5324.

Martin Hantschke received a Dipl. Ing. (BA) in Biomedical Engineering from Berufsakademie Bautzen in 2006. Between 2006 and 2016 he worked as an applied Biomedical Engineer in clinical settings. He received his MSc in Biomedical Engineering with Healthcare Technology Management from City, University of London in 2016. His MSc dissertation was on sensing methods in electrophoresis in collaboration with an industrial partner, Genetic Microdevices Ltd (GMD). Martin is currently carrying out research for his PhD at the Research Centre for

Biomedical Engineering at City, University of London, focusing on spectrophotometric and conductive detection of electrophoretically separated carbohydrates. His PhD is part funded by GMD.

Iasonas F. Triantis is currently Senior Lecturer at the Research Centre for Biomedical Engineering (RCBE), City, University of London. His main interests include methods and systems for combined electrical and optical neural stimulation; medical diagnostics for mental health patients; impedimetric sensing in electrophoresis; re-configurable multi-electrode arrays for targeted diagnostics and impedance plethysmography. He has designed several analogue integrated circuits that investigate and exploit the spatial properties of specific electrode topologies in electrical bio-interfaces. Previously (2010-12) he was a Senior Researcher at the Electronic and Electrical Engineering Department, UCL, focusing on front end ASICs for electrical impedance tomography (EIT). Between 2005-10 he was a Research Associate at Imperial College focusing on multi-modal neuroprostheses and vagus nerve interfaces. Between 2000-5 he was Research Assistant at UCL, where he received his PhD on implantable neural amplifiers. He received his Meng in Electronic Engineering from UMIST in 2000.